Anti-prothrombin autoantibodies enriched after infection with SARS-CoV-2 and influenced by strength of antibody response against SARS-CoV-2 proteins

Marc Emmenegger[1], Sreedhar Saseendran Kumar[2*], Vishalini Emmenegger[2*], Tomas Malinauskas[3], Thomas Büttner[4], Laura Rose[4], Peter Schierack[5,6], Martin F. Sprinzl[7,8], Clemens J. Sommer[9], Karl J. Lackner[8], Adriano Aguzzi[1#], Dirk Roggenbuck[4,5,6#], and Katrin B. M. Frauenknecht[1,9#&]

[1]Institute of Neuropathology, University of Zurich, CH-8091 Zurich, Switzerland

[2]Department of Biosystems Science and Engineering, ETH Zürich, Basel, Switzerland

[3]Division of Structural Biology, Wellcome Centre for Human Genetics, University of Oxford, Oxford, UK

[4]GA Generic Assays GmbH, Ludwig-Erhard-Ring 3, D-15827 Dahlewitz

[5]Institute of Biotechnology, Faculty Environment and Natural Sciences, Brandenburg University of Technology Cottbus-Senftenberg, 01968 Senftenberg, Germany

[6]Faculty of Health Sciences Brandenburg, University of Technology Cottbus-Senftenberg, 01968 Senftenberg, Germany

[7]Department of Internal Medicine I, University Medical Center of the Johannes Gutenberg-University, Langenbeckstr. 1, 55131, Mainz, Germany.

[8]Institute of Clinical Chemistry and Laboratory Medicine, University Medical Center of the Johannes Gutenberg-University , Langenbeckstr. 1, 55131, Mainz, Germany

[9]Institute of Neuropathology, University Medical Center of the Johannes Gutenberg-University, Langenbeckstr. 1, 55131, Mainz, Germany

[*]contributed equally

[#]shared senior authorship

[&] corresponding author

Abstract

Antiphospholipid antibodies (aPL), assumed to cause antiphospholipid syndrome (APS), are notorious for their heterogeneity and detect phospholipids and phospholipid-binding proteins. The persistent presence of Lupus anticoagulant and/or aPL against cardiolipin and/or β2 glycoprotein I have been shown to be independent risk factors for vascular thrombosis and pregnancy morbidity in APS. aPL production is thought to be triggered by – among other factors – viral infections, though infection-associated aPL have mostly been considered non-pathogenic. Recently, the potential pathogenicity of infection-associated aPL has gained momentum since an increasing number of patients infected with Severe Acute Respiratory Syndrome Coronavirus 2 (SARS-CoV-2) has been described with coagulation abnormalities and hyperinflammation, together with the presence of aPL. Here, we present data from a multicentric, mixed-severity study including three cohorts of individuals who contracted SARS-CoV-2 as well as non-infected blood donors. We simultaneously measured 10 different criteria and non-criteria aPL (IgM and IgG) by using a line immunoassay. Further, IgG antibody response against three SARS-CoV-2 proteins was investigated using tripartite automated blood immunoassay technology. Our analyses revealed that selected non-criteria aPL were enriched concomitant to or after an infection with SARS-CoV-2. Linear mixed-effects models suggest an association of aPL to prothrombin (PT) with the strength of the antibody response against SARS-CoV-2 and that it is further influenced by SARS-CoV-2 disease severity and sex of the individuals. In conclusion, our study is the first to report an association between disease severity, anti-SARS-CoV-2 immunoreactivity and aPL against PT in patients with SARS-CoV-2.

Keywords: antiphospholipid antibody, viral infection, COVID-19, SARS-CoV-2, prothrombin antibody, non-criteria aPL, linear mixed-effects models

Introduction

Severe acute respiratory syndrome coronavirus 2 (SARS-CoV-2) was found to elicit a spectrum of autoimmune reactions (Bastard *et al.*, 2020; Wang *et al.*, 2020; Woodruff *et al.*, 2020; Zhou *et al.*, 2020), similar to other viral infections (Bangs, McMichael and Xu, 2006; Tengvall *et al.*, 2019; Kanduc and Shoenfeld, 2020). Patients with severe SARS-CoV-2 infection, some of whom require mechanical ventilation in specialised hospitals wards, have been shown to be at a high risk of developing thrombotic vessel occlusion (Helms *et al.*, 2020). Notably, ischemic events such as stroke have been generally linked with infection, in particular infections affecting the respiratory tract (Sebastian, Stein and Dhamoon, 2019). Along these lines, large-artery ischemic stroke has been identified not only in patients in the current SARS-CoV-2 outbreak (Oxley *et al.*, 2020) but also in 2004 with SARS-CoV-1 (Umapathi *et al.*, 2004).

An association of antiphospholipid antibodies (aPL), mainly of the IgA type, and multiple cerebral infarctions has been reported (Zhang *et al.*, 2020), linking SARS-CoV-2 to a systemic autoimmune disease—the antiphospholipid syndrome (APS) (Taha and Samavati, 2021). Infection-induced non-criteria aPL (Radin *et al.*, 2020) could rise in a transient manner and may reflect a non-pathogenic epiphenomenon. Conversely, aPL extracted from SARS-CoV-2 infected patients were reported to induce an accelerated hypercoagulation via activation of neutrophils and release of neutrophil extracellular traps (NETs) that points to a pathogenic role of aPL in SARS-CoV-2 infected individuals (Zuo *et al.*, 2020). The hypercoagulable state (Violi *et al.*, 2020) with platelet activation, endothelial dysfunction, increased circulating leukocytes, as well as cytokines and fibrinogen in these patients might be the result of an acquired thrombophilia, as described for patients with APS (Miyakis *et al.*, 2006).

To our knowledge, the relationship between criteria and non-criteria aPL and the strength of the antibody response triggered upon infection with SARS-CoV-2 has not been extensively studied. We therefore investigated three cohorts of individuals who contracted SARS-CoV-2 as well as non-infected blood donors in a multi-centre, mixed-severity study. aPL were measured using an established line immunoassay, including criteria aPL against cardiolipin (CL) and β2-glycoprotein I (β2) as well as non-criteria aPL detecting phosphatidic acid (PA), phosphatidylcholine (PC), phosphatidylethanolamine (PE), phosphatidylglycerol (PG), phosphatidylinositol (PI), phosphatidylserine (PS), prothrombin (PT), and annexin V (AnV), respectively. Additionally, we used the tripartite automated blood immunoassay (TRABI) technology (Emmenegger *et al.*, 2020) to investigate anti-SARS-CoV-2 IgG in these cohorts. Overall, our data indicate that PT IgM aPL emerge

proportional to the strength of the antibody response elicited against SARS-CoV-2 proteins, with disease severity and sex as additional contributors.

Methods and Materials

Cohort of patients, convalescent individuals, and healthy blood donors

For this study, we included serum and heparin plasma samples from individuals from Brandenburg/Saxony area, Germany, the University Medical Center Mainz, Mainz, Germany, and the University Hospital Zurich, Zurich, Switzerland. All experiments and analyses involving samples from human donors were conducted with the approval of the local ethics committee (BASEC-Nr. 2020-01731, KEK Zurich; EK2020-16, BTU Cottbus-Senftenberg; reference number 2020-14988-2, ethics committee of the state medical association of Rhineland-Palatinate), in accordance with the provisions of the Declaration of Helsinki and the Good Clinical Practice guidelines of the International Conference on Harmonisation.

Measurement of autoantibodies against criteria and non-criteria phospholipid and phospholipid-related antigens

Line immunoassays (LIA; GA Generic Assays GmbH, Dahlewitz, Germany) for the detection of criteria and non-criteria antiphospholipid antibodies were used as previously described (Nalli *et al.*, 2018; Thaler *et al.*, 2019). Briefly, serum and plasma samples were analysed for IgG and IgM autoantibodies against CL, PA, PC, PE, PG, PI, PS, AnV, β2, and PT, according to the manufacturer's recommendations. Diluted samples (1:33, in 10 mM TRIS with 0.1% Tween-20) were transferred onto LIA stripes, incubated for 30 min at room temperature (RT) while shaking. A 20 min wash step with 1 ml wash buffer (10 mM TRIS with 0.1% Tween-20) was used to remove unbound or loosely attached unspecific components from the LIA stripes. HRP-conjugated anti-human IgM or IgG were incubated for 15 min at RT to bind to autoantibodies. After a subsequent wash step, 500 µl of tetramethylbenzidine (TMB) were added to each LIA stripes as a substrate followed by drying the stripes for at least 30 min at RT. Optical density (OD) of processed strips were analysed densitometrically using a scanner and the corresponding evaluation software, Dr. Dot Line Analyzer (GA Generic Assays GmbH, Dahlewitz, Germany) with a grayscale calibration card for standardization provided with the kit. The cutoff of 50 OD units was determined by calculating the 99th percentile of 150 apparently healthy individuals as recommended by the international classification criteria for aPL testing and Clinical and Laboratory Standards Institute (CLSI) guideline C28-A3 (Roggenbuck *et al.*, 2016; Nalli *et al.*, 2018). Matched plasma and serum samples from randomly selected fully anonymised patients with reported aPL-positivity were used to investigate possible differences in aPL

115 pattern detected by LIA. A linear regression was performed and the Pearson correlation coefficient and R^2 were calculated, along with Bland-Altman analysis to determine possible bias between serum and plasma measurements.

High-throughput SARS-CoV-2 serology using TRABI technology

ELISA-based serology was carried out as previously described (Emmenegger *et al.*, 2020). In brief,
120 high-binding 1536-well plates (Perkin Elmer, SpectraPlate 1536 HB) were coated on the CertusFlex dispenser (Fritz Gyger AG) with 3 µL/well 1 µg/mL SARS-CoV-2 spike ectodomain (S), receptor binding domain (RBD), and nucleocapsid protein (NC) in PBS at 37 °C for 1 h, followed by 3 washes with PBS 0.1% Tween-20 (PBS-T) using Biotek El406 and by blocking with 10 µL 5% milk in PBS-T for 1.5 h. Serum or plasma samples were diluted in sample buffer (1% milk in PBS-T) and dispensed using
125 acoustic dispensing technology employing the ECHO 555 (Labcyte). Thereby, we serially diluted the samples in a range between 1:50-1:6,000, at an assay volume of 3 µL/well. After the sample incubation for 2 h at RT, the wells were washed five times with wash buffer and the presence of IgGs directed against above-defined SARS-CoV-2 antigens were detected using an HRP-linked anti-human IgG antibody (Peroxidase AffiniPure Goat Anti-Human IgG, Fcγ Fragment Specific, Jackson, 109-035-
130 098, at 1:4000 dilution in sample buffer), at a volume of 3 µL/well. The samples were then incubated for one hour at RT and subsequently washed three times with PBS-T. Finally, TMB was added using the syringe dispenser on the MultifloFX (BioTek) at the same assay volume as before, plates were incubated for three minutes at RT, and 3 µL/well 0.5 M H_2SO_4 were added to stop the chromogenic reaction. The absorbance at 450 nm was measured in a plate reader (Perkin Elmer, EnVision) and the
135 inflection points of the sigmoidal binding curves, i.e. p(EC50) values of the respective sample dilution, were determined using the custom designed fitting algorithm referred to earlier (Emmenegger *et al.*, 2020).

The assessment of matrix effects of plasma or serum was conducted on patient-matched samples from randomly selected fully anonymised hospital patients (of unknown SARS-CoV-2 vaccination
140 status) using the same pipeline. Plasma/serum dilutions ranging from 1:100-1:72,900 were conducted in technical duplicates and the results were visualised in GraphPad Prism. A linear regression was performed and the Pearson correlation coefficient and R^2 were calculated, along with Bland-Altman analysis to determine possible bias between serum and plasma measurements.

Exploratory data analysis

145 Pair-wise non-parametric statistical testing was performed to assess differences between controls (non-infected) and SARS-CoV-2 infected individuals. Statistical testing was carried out using MATLAB

(MathWorks). Fisher's exact test was performed with two-tailed probability (95% confidence interval, i.e. α-level = 0.05) to detect differential distributions of positives/negatives between two groups. Mann-Whitney/Wilcoxon rank-sum test was performed on groups with significant differences in the Fisher's exact test to assess whether ODs between the two conditions (non-infected/infected) derive from different populations and a Benjamini-Hochberg post-hoc test (Groppe, 2021) was applied to account for multiple comparisons. Two-sample Kolmogorov-Smirnov test was used to test for differences in the age distributions between the control and SARS-CoV-2 infected groups. Principal component analysis (PCA) and heatmaps were generated in MATLAB (version 9.10). UMAPs were computed using the umap (https://CRAN.R-project.org/package=umap) package in R (version 4.03) using default configuration parameters and plotted using ggplot2.

Development and application of linear fixed-effects and mixed-effects models

We used a linear regression model (fixed-effects) to describe the relationship between a response variable, y, (e.g., β2 or PT IgM) and one or more independent variables, X_i. The independent variables were a mix of continuously valued covariates (e.g., PC1-SARS-CoV-2-IgG, age, days post onset of symptoms) and categorical factors (sex, severity score, test positivity). A linear model of the following form was considered:

$$y = \beta_0 + \beta_1 X_1 + \cdots \beta_n X_n + \varepsilon$$

where ε is the random error.

Least square estimates of the regression coefficients, β_0, $\beta_1, \ldots \beta_n$, were computed using the QR decomposition algorithm.

We developed mixed-effects models as an extension of our fixed-effects models. Here, the regression coefficients could vary with respect to one or more grouping variables. In addition to the fixed-effects, these models included random effects associated with individual experimental units drawn at random from a population. Linear mixed-effects models (LMM) of the following form were considered:

$$y = X\beta + Zb + \varepsilon$$

where y is the response variable; X and Z are fixed and random effect design matrices. β is a p-by-1 fixed-effects vector while b is a q-by-1 random effects vector and p, q here refer to the number of fixed and random effects respectively in the model. The random effects vector, b and the random error term ε were assumed to have the following prior distributions:

$b \sim N\left(0, \sigma^2 D(\theta)\right)$ and $\varepsilon \sim N(0, \sigma_\varepsilon^2 I)$

D is a positive semidefinite matrix parametrized by a variance component vector θ. I is the identity matrix, and σ_ε^2 the residual variance. Mixed-effects models were fitted using the maximum likelihood method.

Model development and variable selection was performed using a manual forward step-up procedure. Starting from a constant model, at each step, we explored an alternative model by adding variables – one at a time – either as a fixed or a random effect. The relative quality of the revised model was assessed using the Akaike Information Criterion (AIS), log likelihood and adjusted R^2. The revised model was retained only if it passed a likelihood ratio test at an α-level of 0.05. The null hypothesis for the test was that the observed response is generated by the simpler model.

Protein similarity analysis between SARS-CoV-2 Spike and human prothrombin

Amino acid sequences were aligned using EMBOSS Matcher and LALIGN (Madeira *et al.*, 2019). Structures were analysed and visualized using the PyMOL Molecular Graphics System, Version 2.3.2 by Schrödinger, LLC (https://pymol.org/2/).

Results

Multi-centre, mixed severity study cohort

Non-infected blood donors (controls, n=20) and samples from individuals who had an RT-qPCR-confirmed SARS-CoV-2 infection (n=75 samples, from 70 individuals, with 5 repeat samples) were included in our study. Non-infected blood donors had a median age of 47 (interquartile range (IQR): 33-55) years, with 45% of individuals being of female and 55% of male sex (**Table 1** and **Fig. S1**). Individuals who contracted SARS-CoV-2 had a median age of 56 (IQR: 47-70) years and a female-to-male ratio of 41:59.

Twenty-two individuals with a history of SARS-CoV-2 infection were sampled in Brandenburg/Saxony area, Germany, at 59 (IQR:57-87) days post onset (DPO) of symptoms (**Table 2**). They had a severity score of 1, which may include symptoms such as anosmia, fever, fatigue, or headache but did not require hospitalization. The cohorts from University Medical Center Mainz (Mainz), Germany (n=27, of whom 22 were unique patients whereof 5 patients had repeat samples) and University Hospital Zurich (Zurich), Switzerland (n=26) were cohorts of patients hospitalized due to COVID-19, with severity scores 2 (hospitalization without requiring oxygen supplementation), 3 (hospitalization requiring oxygen supplementation), and 4 (hospitalization with treatment in the intensive care unit (ICU), mostly including ventilation). The median DPO of symptom for Mainz and Zurich were 13 (IQR: 6-20) and 12 (IQR: 8-15) days, respectively, reflecting earlier time points that still include the acute phase of the infection, unlike for the 22 convalescent individuals who never required hospitalization and were sampled at later timepoints.

Exploratory analyses indicate association of SARS-CoV-2 infection with autoantibodies against β2-glycoprotein I, and prothrombin.

We used an extended IgG and IgM panel of the LIA (Nalli *et al.*, 2018; Thaler *et al.*, 2019) to measure autoantibodies against criteria and non-criteria aPL, including CL, PA, PC, PE, PG, PI, PS, AnV, β2, and PT, in heparin plasma and serum samples of SARS-CoV-2 infected individuals and non-infected controls. For the individuals pertaining to the Zurich cohort, the panel could be applied only to the measurement of IgM aPL due to insufficient sample volume. We assessed the consistency of LIA using matched serum and plasma samples of one patient with reported aPL positivity as well as of a serum sample of one patient with high aPL titer spiked at 1:2 and 1:5 into aPL negative serum and plasma. We found the same pattern of IgM and IgG aPL-positivity in both matched serum and plasma samples as well as in spiked serum and plasma samples, with a Pearson correlation coefficient of 0.9974 (95% confidence intervals: 09611-1.034) and R^2 of 0.9813 (**Fig. S2A**). Bland-Altman analysis

indicated a bias of -2.717 (95% confidence interval: -17.53-12.1) (**Fig. S2B**), suggesting that both serum as well as plasma samples behave in a comparable manner without introducing bias in the
225 subsequent analyses.

We first aimed to gain insights into the reactivity profile by looking at all data in an exploratory manner. We therefore generated a heatmap of the respective IgM (**Fig. 1A**) and IgG aPL profiles (**Fig. 1B**). IgG aPL were typically absent and only rarely close to or above the threshold of OD ≥ 50, a cutoff determined previously by calculating the 99th percentile of 150 apparently healthy individuals
230 (Roggenbuck *et al.*, 2016; Nalli *et al.*, 2018), in both non-infected controls and SARS-CoV-2 infected individuals. IgM aPL titres were generally higher than the corresponding IgGs. PC, PE, and PG IgM aPL did not show any reactivity (median OD 0, for all the three antibodies), with none (PC IgM) or one (PE and PG IgM) individual having values above threshold. Conversely, IgM aPL against CL, PA, PI, PS, AnV, β2, and PT showed a heterogeneous pattern with titres in both the non-infected controls as
235 well as the SARS-CoV-2 infected individuals.

We then investigated whether the overall IgM or IgG aPL profiles were distinct between the SARS-CoV-2 infected individuals and the non-infected controls. We used Uniform Manifold Approximation and Projection (UMAP) to reduce the dimensionality of the dataset while preserving the maximum variability, accounting for potential nonlinear relationships. Neither IgM (**Fig. S2C**) nor IgG profiles
240 (**Fig. S2D**) displayed clear clusters, suggesting that possible differences between non-infected controls and SARS-CoV-2 infected individuals could not be explained in the feature space and require a more granular analysis. On the positive side, the absence of distinct clusters suggests that SARS-CoV-2 infection does not lead to a global and broad dysregulation of aPL.

We subsequently categorised IgM and IgG aPL data according to an OD threshold of 50, with values ≥
245 50 considered positive, and values < 50 negative. Using Fisher's exact test, we found significant distributional differences between non-infected controls and SARS-CoV-2 infected individuals for AnV IgM (p-value = 0.0026), β2 IgM (p-value = 0.0012), and PT IgM (p-value = 0.0052) (**Fig. 1C**) but for none of the IgGs (**Fig. 1D**). To further increase the stringency of our analysis, we subjected AnV, β2, and PT IgM to the Wilcoxon rank sum test, followed by the Benjamini-Hochberg correction for
250 multiple comparisons. Here, we aimed to infer whether the probability of an OD value randomly drawn from the control group being greater than one drawn from the infected population was higher than chance level (α-level = 0.05), considering the entire distribution of data without setting a cutoff. We identified significant distributional changes for β2 (p-value = 0.005), and PT (p-value = 0.005) IgM but not for AnV IgM (p-value = 0.13, i.e., non-significant). Thus, only β2 and PT IgM displayed
255 statistical significance when applying both criteria, indicating robust SARS-CoV-2 associated changes.

We further evaluated these changes in the light of potentially confounding factors when performing pair-wise testing. We first performed a stratified analysis of associations between the response variable and each of the potential confounding factors: sex and age. To confirm our findings, we used multivariate regression and a percent change-in-estimate criterion. A 10% change or more is commonly used as an indicator of a confounding effect (Greenland, 2008; VanderWeele, 2019).

We then explored the influence of sex by stratifying the dependent (β2 IgM and PT IgM OD values) and independent variables (infection status or test positivity) by sex. No trends were found between male and female OD values in each group. Males and females were also similarly distributed among non-infected controls and SARS-CoV-2 infected individuals (**Fig. S1B**). These observations suggest that sex is unlikely to be a confounder. We confirmed this using multivariate regression. Briefly, an ordinary least square regression model was fitted between OD values and infection status. The estimate of the regression coefficient associated with SARS-CoV-2 positivity was highly significant (p-value = 0.008 for PT IgM and 0.001 for β2 IgM). We then added sex as an additional independent variable to the regression equation while observing the change in estimate of the coefficient associated with SARS-CoV-2 positivity. The percent change in the coefficient estimate was less than 4% for both β2 and PT IgM. Hence, we ruled out sex as a confounding factor in our analysis.

We next assessed the confounding effect of age in the comparisons between non-infected and SARS-CoV-2-infected groups (see **Fig. S1A**). Although the age distribution varied between the control and SARS-CoV-2 infected groups (p-value=0.009, two-sample Kolmogorov-Smirnov test), we found no significant correlations between age and (β2 or PT IgM) OD values, either overall, or within the non-infected and SARS-CoV-2-infected groups. Moreover, we discovered that the estimate of the coefficient associated with positivity remained stable when age was added as an additional covariate. The percent change in estimate was less than 5% for both β2 and PT IgM. Hence, age was also ruled out as a confounder in our analysis.

In sum, our data suggests that β2 as well as PT IgM values were upregulated as a function of infection with SARS-CoV-2. An overview of distributional effects including both test statistics used is provided in **Table 3**.

Titre determination of antibodies directed against three SARS-CoV-2 proteins using the TRABI technology.

The clinical picture of SARS-CoV-2 infection is diverse (Gavriatopoulou *et al.*, 2020; Grasselli *et al.*, 2020), the manifestation of first symptoms is highly individual, and its documentation dependent on the governance of the clinical department or the clinician. We have therefore aimed to obtain

additional data by determining the respective SARS-CoV-2 antibody titres using the TRABI technology (Emmenegger *et al.*, 2020), to better characterise the immune profile. First, we analysed patient-
290 matched serum and plasma samples to assess whether its matrix would lead to discordant results. The binding curves (**Fig. S3A**) as well as the resulting p(EC50) values, i.e., antibody titres, were highly congruent (**Fig. S3B**), with a Pearson correlation coefficient of 0.9942 (95% confidence interval: 0.9865-0.9975) and R^2 of 0.9885. The same data was plotted as difference in p(EC50) of serum and plasma and their average (Bland-Altman plot). The calculated bias was extremely low (0.01976,
295 standard deviation: 0.1361) and all data points but two, at very low p(EC50) values, resided within the 95% confidence intervals (-0.2471 to 0.2866), displayed in **Fig. S3C**. This suggested that IgG titres derived from both sample types are comparable. Since the SARS-CoV-2 antibody titres were already available for the cohort from Zurich (published in (Emmenegger *et al.*, 2020)), we measured IgG antibodies against the SARS-CoV-2 spike ectodomain (S), its receptor-binding domain (RBD), and the
300 nucleocapsid protein (NC), in all additional individuals in this study, including the non-infected controls. To this end, eight dilutions (range: 1:50-1:6,000) per sample and antigen were conducted using acoustic dispensing technology and the values were fitted with a logistic regression whereby the p(EC50) was derived, as previously shown (Emmenegger *et al.*, 2020). We thus obtained matched SARS-CoV-2 IgG titres and LIA results, for all samples and all cohorts. We then visualised the
305 respective titres in a heatmap (**Fig. 2A**). Visibly, some of the individuals infected with SARS-CoV-2 displayed titre values in the range of the non-infected controls, most likely because IgG seroconversion had not yet occurred at the time point of sampling. However, the overall separation between non-infected controls and individuals who contracted SARS-CoV-2 was obvious when applying UMAP (**Fig. S3D**).

310 We next illustrated the apparent multicollinearity of the IgG antibody response among S, RBD, and NC (**Fig. 2B**) and applied principal component analysis (PCA), to obtain linear combinations. The first principal component (PC), named PC1-SARS-CoV-2-IgG, accounted for 90.9% (second PC: 7.2%, third PC: 1.9%) of the variability contained within the p(EC50) titres and could therefore be reasonably employed to represent the IgG response against SARS-CoV-2 proteins as a composite metric,
315 explaining most of the variability, in subsequent analyses.

Linear mixed-effects model corroborates the relationship between SARS-CoV-2 infection and aPL against prothrombin and is associated with strength of the antibody response, disease severity, and sex.

Autoantibody responses concomitant to or following a viral infection could be driven by many
320 parameters, including the strength of the specific immune response to components of the viral

pathogen. Some of these features are supposedly independent, others inter-dependent, and the hierarchy of the contributors is unclear, suggesting mixed effects. Aiming to further investigate the relationship between infection to SARS-CoV-2 and IgM aPL against β2 and PT, we therefore chose to utilise a linear mixed-effects model (LMM). Such models allow us to analyse heterogeneous hierarchical data i.e., data that could vary, or may be grouped by multiple factors with observations across groups exhibiting potentially complex association structures (West *et al.*, 2014). By accounting for correlations among observed variables LMMs enable us to study the variation of a dependent variable in terms of components corresponding to each level of the hierarchy (Galecki and Burzykowski, 2013). Though LMMs make assumptions on the distributions of residuals and random effects, they are remarkably robust to violations of these assumptions (Schielzeth *et al.*, 2020). For these reasons, they find broad application in life science, psychology, and medicine (see e.g. Jaeger, 2008; Aarts *et al.*, 2014; Brown and Prescott, 2015; Magezi, 2015).

Essentially, the main assumption is that a dependent variable is linearly related to fixed or random factors, with the fixed effects modelling the mean of the dependent variable and the random effects its variability within and between each grouping variable. Along these lines, while so far, our data indicated that an infection with SARS-CoV-2 could influence IgG or IgM aPL levels, we made no assumptions over which additional parameters would be influential. We have therefore chosen a stepwise exploratory approach.

First, using all values available and without segregating the non-infected controls and the SARS-CoV-2 infected individuals, we inspected β2 and PT IgM aPL levels as a function of PC1-SARS-CoV-2-IgG levels, looking at sex, disease severity, DPO, and age (**Fig. 3A**). Visually, data seemed indicative of a potential effect of sex on PT IgM levels. Additionally, severity might be partially predictive of β2 and PT IgM levels, while DPO and age did not display a perceptible linear relation. As a point of caution, the distributions of β2 and PT IgM were skewed, with an enrichment at OD 0 as well as at ca. OD 40, leading to the appearance of a quasi-binomial distribution (**Fig. 3A**). To account for this, individuals with OD < 5 for a given antigen were removed from the subsequent regression analysis. Thus, we aimed to specifically investigate the most important factors regulating the presence, and not the absence, of IgM aPL against β2 and PT. Generally, we first fitted an ordinary least square regression model, then added variables as fixed and as mixed effects and assessed general model parameters (Akaike Information Criterion (AIC), log-likelihood, adjusted R^2, and the p-value of the likelihood ratio) and whether the slopes or intercepts improved. While we observed that the fits for both β2 and PT improved when including PC1-SARS-CoV-2-IgG for prediction, none of the additional variables added as a fixed- or mixed-effect were informative in predicting the best fit for β2 IgM. β2 IgM

values, in general, were not found to be well explained by a linear model, fixed or mixed. Even if the
355 inclusion of DPO seemed to be informative according to the likelihood ratio, it caused a change in the estimate of PC1-SARS-CoV-2-IgG by 55% and worsened the adjusted R^2. Thus, DPO should be interpreted as a confounder for β2 IgM, in this context. Conversely, the inclusion of sex proved informative on the intercept as well as the slope for PT IgM, and the information contained in DPO further refined the model, in addition to PC1-SARS-CoV-2-IgG (see **Table S1**). The best fits for both β2
360 as well as PT IgM are plotted in **Fig. 3B**. Although the mixed-effect model already accounted for differences between the acute and the convalescent groups in terms of DPO, we additionally removed the convalescent individuals from the analysis to subject the finding to scrutiny. The best fit for PT IgM included PC1-SARS-CoV-2-IgG and sex (see **Table S2**), as above, and is plotted in **Fig. 3C**. Thus, the above identified relation is consistent after the exclusion of convalescent individuals.

365 Finally, we investigated the relationship between PC1-SARS-CoV-2-IgG and β2 or PT IgM levels strictly in the fraction of individuals who contracted SARS-CoV-2, using a similar approach to the one described above (see **Table S3**). This is an important addition as we needed to ensure that the weak antibody score, PC1-SARS-CoV-2-IgG, characteristic for non-infected individuals (see **Fig. 2A** and **3A**) is not biasing the analyses of those individuals who contracted SARS-CoV-2. While β2 IgM levels did
370 not display robust improvements upon inclusion of age, sex, DPO, disease severity (in line with the model that includes the non-infected controls), or PC1-SARS-CoV-2-IgG (opposed to the model that includes the non-infected controls), the best fit model indicated that the addition of the composite metric (PC1-SARS-CoV-2-IgG), the severity score, and sex were informative to predict PT IgM levels. The best models for β2 and PT IgM, in the absence of non-infected controls, are shown in **Fig. 3D**. We
375 thus conclude that PT IgM aPL levels are mostly associated with the strength of the antibody response elicited against SARS-CoV-2 proteins tested here and are further influenced by disease severity and sex.

Anti-PT autoimmunity is likely not mediated by cross-reactive IgM antibodies to SARS-CoV-2 Spike protein

380 Given aPT antibodies are enriched after SARS-CoV-2 infection, we asked whether SARS-CoV-2 Spike could have elicited the production of cross-reactive antibodies of the IgM isotypes, recognising both Spike and PT. To address this question, we identified similarities between Spike and PT amino acid sequences using two methods (EMBOSS Matcher and LALIGN) (Madeira *et al.*, 2019). Furthermore, to assess whether shared sequences could be recognized by antibodies, we mapped identified
385 sequences onto PT and Spike structures (Pozzi *et al.*, 2016; Huo *et al.*, 2020). Although two proteins differ in their domain architecture, structural analyses revealed four regions of Spike that are similar

to PT (sequence identity 27–35% for 21–76 aligned residues; **Fig. 4A**). All four regions encompass residues that are exposed on protein surfaces and, thus, could be recognised by antibodies (**Fig. 4B** and **C**). However, region 1 contains an N-linked glycosylation site that could interfere with the Spike/PT–antibody interactions. Region 2 contains the PRTF motif shared by two proteins, but they adopt rather different conformations (**Fig. 4D**). Regions 3 and 4 lack continuous stretches of identical residues that are longer than 2–3 amino acids. While detailed analyses of the degree of convergence of complementarity-determining regions (CDRs) between antibodies against SARS-CoV-2 Spike and human PT may be informative, prothrombin and Spike share rather limited similarity and, thus, seem less likely to be recognised by the same antibody.

Discussion

Here, we studied patients who contracted SARS-CoV-2 for the occurrence of aPL, in three cohorts originating from three different centers, with mixed disease severity scores. In general, we have chosen a largely data-driven approach. While our main hypothesis was that an infection with SARS-CoV-2 may enhance IgG and/or IgM aPL levels, we had no prior assumption regarding parameters that could potentially be influential. We have therefore collected available parameters and, following a first assessment of which aPL are altered and, thus, worth pursuing, analysed them in a stepwise exploratory manner. Moreover, we established their relationship using linear mixed-effects models, aiming to identify the parameters, and their combinations, that best predict aPL levels. Lastly, we speculated that cross-reactive IgM antibodies against the SARS-CoV-2 Spike protein could trigger autoimmunity against prothrombin.

We first measured IgG and IgM aPL against criteria (CL and β2) and non-criteria antigens (PA, PC, PE, PG, PI, PS, PT, AnV) and then supplemented our dataset with detailed information on the antibody status of all participants by measuring the presence of IgG directed against SARS-CoV-2 S, RBD, and the NC protein. Our cohorts comprised patients presenting with uncomplicated, mild, moderate and severe disease courses of COVID-19 as well as healthy blood donors who had not contracted SARS-CoV-2. To characterise these patients, we availed of features such as aPL levels, SARS-CoV-2 antibody titres, disease severity, basic demographic information (sex and age), and DPO of sample.

Prior knowledge suggests the presence of a plethora of aPL, including LA, in COVID-19 (Taha and Samavati, 2021). Moreover, severe disease courses, including COVID-19-associated coagulopathy (CAC) are reminiscent of so-called catastrophic APS (CAPS), which features venous and/or arterial vascular thrombosis as well as pulmonary and heart damage with endothelial injury and microthrombosis (Goshua *et al.*, 2020; Iba *et al.*, 2020, 2021; Varga *et al.*, 2020; Maccio *et al.*, 2021). CAPS is an utterly devastating disease with around 30% mortality (Cervera *et al.*, 2009), in which patients usually develop multiple organ damage over a short period of time (Asherson and Cervera, 1994; Cervera, 2010). CAPS appears to be linked to infections in the first place in nearly half of the patients (Cervera *et al.*, 2009). Uncontrolled complement activation may further contribute to an unfavourable disease course (Cervera *et al.*, 2009).

In our study, we pursued two main objectives. We (1) aimed to provide further evidence for the occurrence of aPL as a result of infection with SARS-CoV-2 and (2) aimed to identify potential correlates. Indeed, we found that, globally, IgM or IgG levels are increased upon infection with SARS-CoV-2, with 66% of individuals having aPL against ≥1 antigen (non-infected controls: 15%), 40%

against ≥2 antigens (non-infected controls: 0%), and 21.3% against ≥3 antigens (non-infected
430 controls: 0%), using a threshold of OD ≥ 50. Thus, the prevalence of aPL was higher in our study than previously reported (Borghi *et al.*, 2020; Zuo *et al.*, 2020; Cristiano *et al.*, 2021; Taha and Samavati, 2021), despite not including LA in the measurements, and in spite of omitting IgA aPL. Importantly, we detected significant distributional changes between non-infected controls and SARS-CoV-2-infected individuals for IgM aPL against AnV, β2, and PT using Fisher's exact test (p-values < 0.01),
435 and for β2, and PT using Wilcoxon rank sum test (p-values < 0.01 after Benjamini-Hochberg correction). Hence, in our study, we found an association of IgM, and not of IgG, aPL with SARS-CoV-2 infection.

Polyreactive circulating IgM antibodies can bind to membrane phospholipids (Fu *et al.*, 2007) and are supposed to have a protective function (Briles *et al.*, 1981). In contrast, such antibodies may not only
440 clear the system from damaged cells but may also drive subsequent cell damage by additional complement activation (Narang *et al.*, 2017). In the context of infection with SARS-CoV-2, increased cell death/apoptosis has been described (Li *et al.*, 2020). Specifically, phospholipid-rich pulmonary surfactant leakage (Fessler and Summer, 2016) following SARS-CoV-2-induced pulmonary cell necrosis may further trigger the rise of aPL. AnV, β2, and PT IgM aPL are enriched after SARS-CoV-2
445 infection and may last longer than three months, at least in a subset of COVID-19 patients (Vollmer *et al.*, 2021). AnV aPL have been linked to a (pro)thrombotic state in several diseases including sickle cell disease (Sater *et al.*, 2011) and APS (Zhang *et al.*, 2017). Additionally, AnV IgG or IgM were associated with higher occurrence of pulmonary arterial hypertension and were detectable throughout a 2-year follow-up in patients with systemic sclerosis (Horimoto *et al.*, 2020). β2 and PT
450 aPL were reported to cause LA (1) via direct interaction of β2 aPL with FV and activation by FXa and (2) via PT aPL competition with FXa for PL binding sites (Noordermeer *et al.*, 2021), actions which may account for the higher prevalence of LA described in patients with COVID-19 (Taha and Samavati, 2021). However, a very recent study indicated LA as a transient phenomenon during SARS-CoV-2 infection (Vollmer *et al.*, 2021). We then decided to focus on β2 and PT IgM aPL and asked
455 what features were predictive of their occurrence. To this end, we started with an ordinary least square regression model, then added variables as fixed and random effects in multiple linear regressions and assessed general model parameters (AIC, log-likelihood, adjusted R^2, and the p-value of the likelihood ratio) and searched whether the slopes or intercepts improved. We accounted for collinearity of antibodies against SARS-CoV-2, thus, intrinsic correlation, by using the first PC derived
460 from linear combinations of S, RBD, and NC p(EC50) values (PC1-SARS-CoV-2-IgG). While β2 IgM aPL levels were found to be correlated with the strength of the anti-SARS-CoV-2 antibody response, none of the other features showed significant predictive power. Conversely, PT IgM aPL were best

predicted by the strength of the antibody response against SARS-CoV-2 (PC1-SARS-CoV-2-IgG) but also by sex as well as disease severity in patients who contracted SARS-CoV-2.

The detection of antibodies against negatively charged phospholipids and plasma proteins other than CL and β2 may have diagnostic and/or therapeutic consequences. Such aPL e.g., against members of the coagulation cascade like PT or against the PS/PT complex have been described in patients with unprovoked venous thromboembolism (Ho and Rigano, 2020) seronegative APS (Zohoury *et al.*, 2017), and SLE (Tsutsumi *et al.*, 2006). Although aPL against PT and PS/PT significantly correlate with each other, conformational changes after PT binding to PS may expose different epitopes for aPL binding (Tsutsumi *et al.*, 2006). Both aPL require different reaction environments for their specific detection (Roggenbuck *et al.*, 2016). Still, the pathogenicity of these non-criteria (mainly lipid-reactive) aPL associated with SARS-CoV-2 infections is a matter of debate. Recently, a report suggested an association of high-titer aPL (mainly PS/PT) with increased NETosis and more severe respiratory disease in COVID-19 patients (Zuo *et al.*, 2020). In addition, purified IgG from these patients further led to immune dysregulation and thrombosis in mice (Zuo *et al.*, 2020). Thus, non-criteria aPL may have pro-thrombotic potential in humans, even if only transiently present.

Molecular mimicry between a pathogenic entity (e.g. virus, bacteria, fungi) and cofactors such as β2 is one of the mechanisms suggested to cause aPL (Blank *et al.*, 2002). However, our analyses revealed a rather limited similarity between SARS-CoV-2 Spike protein and PT, and thus suggest a more complex mechanism by which aPT antibodies are elicited. The immunological cascade triggered upon infection with SARS-CoV-2 results in a broad autoantibody response (Bastard *et al.*, 2020; Wang *et al.*, 2020; Woodruff *et al.*, 2020), by a detailed mechanism that yet needs to be established. For the generation of aPT specifically, other proteins involved in the processing, cellular entry and infectivity of SARS-CoV-2 could be of relevance. For instance, one may hypothesise that cross-reactivity between PT and TMPRSS2, a transmembrane serine protease (TTSP) essential for SARS-CoV-2 entry into host cells (Koch *et al.*, 2021; Muley *et al.*, 2021) could result in the induction of such antibodies. Recent work further showed that coagulation factors like thrombin cleave SARS-CoV-2 Spike protein and enhance virus entry in cells (Kastenhuber *et al.*, 2021). However, the impact of aPT on these actions is not known and would need further investigation.

In conclusion, our study further emphasizes a potentially pathogenic role of PT IgM aPL in SARS-CoV-2 infected individuals. We find that its levels significantly correlate with the anti-SARS-CoV-2 antibody response elicited upon infection and is additionally influenced by disease severity and sex. Further studies are needed to assess whether only a specific subset of patients (e.g., genetically defined) would be at risk for developing such aPL.

References

Aarts, E., Verhage, M., Veenvliet, J. V., Dolan, C. V. and Van Der Sluis, S. (2014) 'A solution to dependency: Using multilevel analysis to accommodate nested data', *Nature Neuroscience*, 17(4), pp. 491–496. doi: 10.1038/NN.3648.

Asherson, R. A. and Cervera, R. (1994) '"Primary", "Secondary" and Other Variants of the Antiphospholipid Syndrome', *Lupus*, 3(4), pp. 293–298. doi: 10.1177/096120339400300417.

Bangs, S. C., McMichael, A. J. and Xu, X. N. (2006) 'Bystander T cell activation - implications for HIV infection and other diseases', *Trends in Immunology*, 27(11), pp. 518–524. doi: 10.1016/j.it.2006.09.006.

Bastard, P., Rosen, L. B., Zhang, Q., Michailidis, E., Hoffmann, H. H., Zhang, Y., Dorgham, K., Philippot, Q., Rosain, J., Béziat, V., *et al.* (2020) 'Autoantibodies against type I IFNs in patients with life-threatening COVID-19', *Science*, 370(6515). doi: 10.1126/science.abd4585.

Blank, M., Krause, I., Fridkin, M., Keller, N., Kopolovic, J., Goldberg, I., Tobar, A. and Shoenfeld, Y. (2002) 'Bacterial induction of autoantibodies to β2-glycoprotein-I accounts for the infectious etiology of antiphospholipid syndrome', *Journal of Clinical Investigation*, 109(6), pp. 797–804. doi: 10.1172/jci12337.

Borghi, M. O., Beltagy, A., Garrafa, E., Curreli, D., Cecchini, G., Bodio, C., Grossi, C., Blengino, S., Tincani, A., Franceschini, F., *et al.* (2020) 'Anti-Phospholipid Antibodies in COVID-19 Are Different From Those Detectable in the Anti-Phospholipid Syndrome', *Frontiers in Immunology*, 11. doi: 10.3389/fimmu.2020.584241.

Briles, D. E., Nahm, M., Schroer, K., Davie, J., Baker, P., Kearney, J. and Barletta, R. (1981) 'Antiphosphocholine antibodies found in normal mouse serum are protective against intravenous infection with type 3 Streptococcus pneumoniae', *Journal of Experimental Medicine*, 153(3), pp. 694–705. doi: 10.1084/jem.153.3.694.

Brown, H. and Prescott, R. (2015) *Applied Mixed Models in Medicine*. 3rd Editio. Wiley.

Cervera, R. (2010) 'Update on the Diagnosis, Treatment, and Prognosis of the Catastrophic Antiphospholipid Syndrome', *Current Rheumatology Reports*, 12(1), pp. 70–76. doi: 10.1007/s11926-009-0073-6.

Cervera, R., Bucciarelli, S., Plasín, M. A., Gómez-Puerta, J. A., Plaza, J., Pons-Estel, G., Shoenfeld, Y., Ingelmo, M. and Espinos, G. (2009) 'Catastrophic antiphospholipid syndrome (CAPS): Descriptive

analysis of a series of 280 patients from the "CAPS Registry"', *Journal of Autoimmunity*, 32(3–4), pp. 240–245. doi: 10.1016/j.jaut.2009.02.008.

Cristiano, A., Fortunati, V., Cherubini, F., Bernardini, S. and Nuccetelli, M. (2021) 'Anti-phospholipids antibodies and immune complexes in COVID-19 patients: a putative role in disease course for anti-annexin-V antibodies', *Clinical Rheumatology*, pp. 1–7. doi: 10.1007/s10067-021-05580-3.

Emmenegger, M., De Cecco, E., Lamparter, D., Jacquat, R. P. B., Ebner, D., Schneider, M. M., Condado Morales, I., Schneider, D., Dogancay, B., Guo, J., *et al.* (2020) 'Early peak and rapid decline of SARS-CoV-2 seroprevalence in a Swiss metropolitan region', *medRxiv*. doi: 10.1101/2020.05.31.20118554.

Fessler, M. B. and Summer, R. S. (2016) 'Surfactant lipids at the host-environment interface metabolic sensors, suppressors, and effectors of inflammatory lung disease', *American Journal of Respiratory Cell and Molecular Biology*. American Thoracic Society, pp. 624–635. doi: 10.1165/rcmb.2016-0011PS.

Fu, M., Fan, P. S., Li, W., Li, C. X., Xing, Y., An, J. G., Wang, G., Fan, X. L., Gao, T. W., Liu, Y. F., *et al.* (2007) 'Identification of poly-reactive natural IgM antibody that recognizes late apoptotic cells and promotes phagocytosis of the cells', *Apoptosis*, 12(2), pp. 355–362. doi: 10.1007/s10495-006-0581-z.

Galecki, A. and Burzykowski, T. (2013) 'Linear Mixed-Effects Models Using R: A Step-by-Step Approach', in.

Gavriatopoulou, M., Korompoki, E., Fotiou, D., Ntanasis-Stathopoulos, I., Psaltopoulou, T., Kastritis, E., Terpos, E. and Dimopoulos, M. A. (2020) 'Organ-specific manifestations of COVID-19 infection', *Clinical and Experimental Medicine*. Springer Science and Business Media Deutschland GmbH, pp. 493–506. doi: 10.1007/s10238-020-00648-x.

Goshua, G., Pine, A. B., Meizlish, M. L., Chang, C. H., Zhang, H., Bahel, P., Baluha, A., Bar, N., Bona, R. D., Burns, A. J., *et al.* (2020) 'Endotheliopathy in COVID-19-associated coagulopathy: evidence from a single-centre, cross-sectional study', *The Lancet Haematology*, 7(8), pp. e575–e582. doi: 10.1016/S2352-3026(20)30216-7.

Grasselli, G., Zangrillo, A., Zanella, A., Antonelli, M., Cabrini, L., Castelli, A., Cereda, D., Coluccello, A., Foti, G., Fumagalli, R., *et al.* (2020) 'Baseline Characteristics and Outcomes of 1591 Patients Infected with SARS-CoV-2 Admitted to ICUs of the Lombardy Region, Italy', *JAMA - Journal of the American Medical Association*, 323(16), pp. 1574–1581. doi: 10.1001/jama.2020.5394.

Greenland, S. (2008) 'Invited commentary: Variable selection versus shrinkage in the control of

multiple confounders', *American Journal of Epidemiology*. Am J Epidemiol, pp. 523–529. doi: 10.1093/aje/kwm355.

Groppe, D. (2021) *fdr_bh (MATLAB Central File Exchange)*. Available at: https://www.mathworks.com/matlabcentral/fileexchange/27418-fdr_bh (Accessed: 9 August 2021).

Helms, J., Tacquard, C., Severac, F., Leonard-Lorant, I., Ohana, M., Delabranche, X., Merdji, H., Clere-Jehl, R., Schenck, M., Fagot Gandet, F., *et al.* (2020) 'High risk of thrombosis in patients with severe SARS-CoV-2 infection: a multicenter prospective cohort study', *Intensive Care Medicine*, 46(6), pp. 1089–1098. doi: 10.1007/s00134-020-06062-x.

Ho, W. K. and Rigano, J. (2020) 'Prevalence of autoantibodies directed against prothrombin in unprovoked venous thromboembolism', *Journal of Thrombosis and Thrombolysis*, 49(3), pp. 446–450. doi: 10.1007/s11239-020-02053-3.

Horimoto, A. M. C., De Jesus, L. G., De Souza, A. S., Rodrigues, S. H. and Kayser, C. (2020) 'Anti-Annexin v autoantibodies and vascular abnormalities in systemic sclerosis: A longitudinal study', *Advances in Rheumatology*, 60(1). doi: 10.1186/s42358-020-00140-w.

Huo, J., Zhao, Y., Ren, J., Zhou, D., Duyvesteyn, H. M. E., Ginn, H. M., Carrique, L., Malinauskas, T., Ruza, R. R., Shah, P. N. M., *et al.* (2020) 'Neutralization of SARS-CoV-2 by Destruction of the Prefusion Spike', *Cell Host and Microbe*, 28(3), pp. 445-454.e6. doi: 10.1016/j.chom.2020.06.010.

Iba, T., Levy, J. H., Connors, J. M., Warkentin, T. E., Thachil, J. and Levi, M. (2020) 'The unique characteristics of COVID-19 coagulopathy', *Critical Care*. BioMed Central, pp. 1–8. doi: 10.1186/s13054-020-03077-0.

Iba, T., Warkentin, T. E., Thachil, J., Levi, M. and Levy, J. H. (2021) 'Proposal of the Definition for COVID-19-Associated Coagulopathy', *Journal of Clinical Medicine*, 10(2), p. 191. doi: 10.3390/jcm10020191.

Jaeger, T. F. (2008) 'Categorical data analysis: Away from ANOVAs (transformation or not) and towards logit mixed models', *Journal of Memory and Language*, 59(4), pp. 434–446. doi: 10.1016/J.JML.2007.11.007.

Kanduc, D. and Shoenfeld, Y. (2020) 'From Anti-EBV Immune Responses to the EBV Diseasome via Cross-reactivity', *Global Medical Genetics*, 07(02), pp. 051–063. doi: 10.1055/s-0040-1715641.

Kastenhuber, E. R., Jaimes, J. A., Johnson, J. L., Marisa Mercadante, Frauke Muecksch3, Yiska Weisblum3, Yaron Bram4, Robert E. Schwartz4, 5, G. R. W. L. C. C., Mercadante, M., Muecksch, F.,

Weisblum, Y., Bram, Y., Schwartz, R. E., Whittaker, G. R., *et al.* (2021) 'Coagulation factors directly cleave SARS-CoV-2 spike and enhance viral entry', *bioRxiv*, 53(9), p. 2021.03.31.437960. doi: 10.1101/2021.03.31.437960.

Koch, J., Uckeley, Z. M., Doldan, P., Stanifer, M., Boulant, S. and Lozach, P.-Y. (2021) 'TMPRSS2 expression dictates the entry route used by SARS-CoV-2 to infect host cells', *The EMBO Journal*, 40(16), p. e107821. doi: 10.15252/EMBJ.2021107821.

Li, S., Zhang, Y., Guan, Z., Li, H., Ye, M., Chen, X., Shen, J., Zhou, Y., Shi, Z.-L., Zhou, P., *et al.* (2020) 'SARS-CoV-2 triggers inflammatory responses and cell death through caspase-8 activation.', *Signal transduction and targeted therapy*, 5(1), p. 235. doi: 10.1038/s41392-020-00334-0.

Maccio, U., Zinkernagel, A. S., Shambat, S. M., Zeng, X., Cathomas, G., Ruschitzka, F., Schuepbach, R. A., Moch, H. and Varga, Z. (2021) 'SARS-CoV-2 leads to a small vessel endotheliitis in the heart', *EBioMedicine*, 63. doi: 10.1016/j.ebiom.2020.103182.

Madeira, F., Park, Y. M., Lee, J., Buso, N., Gur, T., Madhusoodanan, N., Basutkar, P., Tivey, A. R. N., Potter, S. C., Finn, R. D., *et al.* (2019) 'The EMBL-EBI search and sequence analysis tools APIs in 2019', *Nucleic Acids Research*, 47(W1), pp. W636–W641. doi: 10.1093/nar/gkz268.

Magezi, D. A. (2015) 'Linear mixed-effects models for within-participant psychology experiments: an introductory tutorial and free, graphical user interface (LMMgui)', *Frontiers in Psychology*, 0(JAN), p. 2. doi: 10.3389/FPSYG.2015.00002.

Miyakis, S., Lockshin, M. D., Atsumi, T., Branch, D. W., Brey, R. L., Cervera, R., Derkesen, R. H. W. M., De Groot, P. G., Koike, T., Meroni, P. L., *et al.* (2006) 'International consensus statement on an update of the classification criteria for definite antiphospholipid syndrome (APS)', *Journal of Thrombosis and Haemostasis*, 4(2), pp. 295–306. doi: 10.1111/j.1538-7836.2006.01753.x.

Muley, V. Y., Singh, A., Gruber, K. and Varela-Echavarria, A. (2021) 'SARS-CoV-2 Entry Protein TMPRSS2 and Its Homologue, TMPRSS4 Adopts Structural Fold Similar to Blood Coagulation and Complement Pathway Related Proteins', *bioRxiv*, p. 2021.04.26.441280. doi: 10.1101/2021.04.26.441280.

Nalli, C., Somma, V., Andreoli, L., Büttner, T., Schierack, P., Mahler, M., Roggenbuck, D. and Tincani, A. (2018) 'Anti-phospholipid IgG antibodies detected by line immunoassay differentiate patients with anti-phospholipid syndrome and other autoimmune diseases', *Autoimmunity Highlights*, 9(1). doi: 10.1007/s13317-018-0106-0.

Narang, A., Qiao, F., Atkinson, C., Zhu, H., Yang, X., Kulik, L., Holers, V. M. and Tomlinson, S. (2017) 'Natural IgM antibodies that bind neoepitopes exposed as a result of spinal cord injury , drive secondary injury by activating complement', *Journal of Neuroinflammation*, 14(1), pp. 1–12. doi: 10.1186/s12974-017-0894-6.

Noordermeer, T., Molhoek, J. E., Schutgens, R. E. G., Sebastian, S. A. E., Drost-Verhoef, S., van Wesel, A. C. W., de Groot, P. G., Meijers, J. C. M. and Urbanus, R. T. (2021) 'Anti-β2-glycoprotein I and anti-prothrombin antibodies cause lupus anticoagulant through different mechanisms of action', *Journal of Thrombosis and Haemostasis*, 19(4), pp. 1018–1028. doi: 10.1111/jth.15241.

Oxley, T. J., Mocco, J., Majidi, S., Kellner, C. P., Shoirah, H., Singh, I. P., De Leacy, R. A., Shigematsu, T., Ladner, T. R., Yaeger, K. A., *et al.* (2020) 'Large-Vessel Stroke as a Presenting Feature of Covid-19 in the Young', *New England Journal of Medicine*, 382(20), p. e60. doi: 10.1056/nejmc2009787.

Pozzi, N., Chen, Z., Di Cera, E., N, P., Z, C. and E, D. C. (2016) 'How the Linker Connecting the Two Kringles Influences Activation and Conformational Plasticity of Prothrombin', *The Journal of biological chemistry*, 291(12), pp. 6071–6082. doi: 10.1074/JBC.M115.700401.

Radin, M., Cecchi, I., Foddai, S. G., Rubini, E., Barinotti, A., Ramirez, C., Seaman, A., Roccatello, D., Mahler, M. and Sciascia, S. (2020) 'Validation of the Particle-Based Multi-Analyte Technology for Detection of Anti-PhosphatidylSerine/Prothrombin Antibodies', *Biomedicines*, 8(12). doi: 10.3390/biomedicines8120622.

Roggenbuck, D., Borghi, M. O., Somma, V., Büttner, T., Schierack, P., Hanack, K., Grossi, C., Bodio, C., Macor, P., von Landenberg, P., *et al.* (2016) 'Antiphospholipid antibodies detected by line immunoassay differentiate among patients with antiphospholipid syndrome, with infections and asymptomatic carriers', *Arthritis Research & Therapy*, 18(1), p. 111. doi: 10.1186/s13075-016-1018-x.

Sater, M. S., Mahdi, N., Al-Absi, I. K., Al-Subaie, A. M., Al-Ola, K., Mohammed, F. A. and Almawi, W. Y. (2011) 'Anti-annexin v IgG and IgM antibodies in sickle cell disease patients with vaso-occlusive crisis', *Annals of Hematology*, 90(9), pp. 1031–1036. doi: 10.1007/s00277-011-1184-5.

Schielzeth, H., Dingemanse, N. J., Nakagawa, S., Westneat, D. F., Allegue, H., Teplitsky, C., Réale, D., Dochtermann, N. A., Garamszegi, L. Z. and Araya-Ajoy, Y. G. (2020) 'Robustness of linear mixed-effects models to violations of distributional assumptions', *Methods in Ecology and Evolution*, 11(9), pp. 1141–1152. doi: 10.1111/2041-210X.13434.

Sebastian, S., Stein, L. K. and Dhamoon, M. S. (2019) 'Infection as a Stroke Trigger: Associations between Different Organ System Infection Admissions and Stroke Subtypes', *Stroke*, 50(8), pp. 2216–

2218. doi: 10.1161/STROKEAHA.119.025872.

Taha, M. and Samavati, L. (2021) 'Antiphospholipid antibodies in COVID-19: A meta-analysis and systematic review', *RMD Open*. BMJ Publishing Group. doi: 10.1136/rmdopen-2021-001580.

Tengvall, K., Huang, J., Hellström, C., Kammer, P., Biström, M., Ayoglu, B., Bomfim, I. L., Stridh, P., Butt, J., Brenner, N., *et al.* (2019) 'Molecular mimicry between Anoctamin 2 and Epstein-Barr virus nuclear antigen 1 associates with multiple sclerosis risk', *Proceedings of the National Academy of Sciences of the United States of America*, 116(34), pp. 16955–16960. doi: 10.1073/pnas.1902623116.

Thaler, M. A., Bietenbeck, A., Steigerwald, U., Büttner, T., Schierack, P., Lindhoff-Last, E., Roggenbuck, D. and Luppa, P. B. (2019) 'Evaluation of the sensitivity and specificity of a novel line immunoassay for the detection of criteria and non-criteria antiphospholipid antibodies in comparison to established ELISAs', *PLoS ONE*, 14(7), p. e0220033. doi: 10.1371/journal.pone.0220033.

Tsutsumi, A., Hayashi, T., Chino, Y., Mamura, M., Goto, D., Matsumoto, I., Ito, S. and Sumida, T. (2006) 'Significance of antiprothrombin antibodies in patients with systemic lupus erythematosus: clinical evaluation of the antiprothrombin assay and the antiphosphatidylserine/prothrombin assay, and comparison with other antiphospholipid antibody assays', *Modern Rheumatology*, 16(3), pp. 158–164. doi: 10.3109/s10165-006-0481-7.

Umapathi, T., Kor, A. C., Venketasubramanian, N., Lim, C. C. T., Pang, B. C., Yeo, T. T., Lee, C. C., Lim, P. L., Ponnudurai, K., Chuah, K. L., *et al.* (2004) 'Large artery ischaemic stroke in severe acute respiratory syndrome (SARS)', *Journal of Neurology*, 251(10), pp. 1227–1231. doi: 10.1007/s00415-004-0519-8.

VanderWeele, T. J. (2019) 'Principles of confounder selection', *European Journal of Epidemiology*, 34(3), pp. 211–219. doi: 10.1007/s10654-019-00494-6.

Varga, Z., Flammer, A. J., Steiger, P., Haberecker, M., Andermatt, R., Zinkernagel, A. S., Mehra, M. R., Schuepbach, R. A., Ruschitzka, F. and Moch, H. (2020) 'Endothelial cell infection and endotheliitis in COVID-19', *The Lancet*. Lancet Publishing Group, pp. 1417–1418. doi: 10.1016/S0140-6736(20)30937-5.

Violi, F., Pastori, D., Cangemi, R., Pignatelli, P. and Loffredo, L. (2020) 'Hypercoagulation and Antithrombotic Treatment in Coronavirus 2019: A New Challenge', *Thrombosis and Haemostasis*, 120(6), pp. 949–956. doi: 10.1055/s-0040-1710317.

Vollmer, O., Tacquard, C., Dieudonné, Y., Nespola, B., Sattler, L., Grunebaum, L., Gies, V.,

Radosavljevic, M., Kaeuffer, C., Hansmann, Y., *et al.* (2021) 'Follow-up of COVID-19 patients: LA is transient but other aPLs are persistent', *Autoimmunity Reviews*, 20(6), p. 102822. doi: 10.1016/j.autrev.2021.102822.

Wang, E. Y., Mao, T., Klein, J., Dai, Y., Huck, J. D., Liu, F., Zheng, N. S., Zhou, T., Israelow, B., Wong, P., *et al.* (2020) 'Diverse Functional Autoantibodies in Patients with COVID-19.', *medRxiv: the preprint server for health sciences*, p. 2020.12.10.20247205. doi: 10.1101/2020.12.10.20247205.

West, B. T., Welch, K. B., Gałecki, A. T. and Gillespie, B. W. (2014) 'Linear mixed models: a practical guide using statistical software', p. 407.

Woodruff, M. C., Ramonell, R. P., Lee, F. E. H. and Sanz, I. (2020) 'Clinically identifiable autoreactivity is common in severe SARS-CoV-2 infection', *medRxiv*. medRxiv. doi: 10.1101/2020.10.21.20216192.

Zhang, S., Wu, Z., Li, J., Wen, X., Li, L., Zhang, W., Zhao, J., Zhang, F. and Li, Y. (2017) 'Evaluation of the clinical relevance of anti-annexin-A5 antibodies in Chinese patients with antiphospholipid syndrome', *Clinical Rheumatology*, 36(2), pp. 407–412. doi: 10.1007/s10067-016-3510-8.

Zhang, Y., Xiao, M., Zhang, Shulan, Xia, P., Cao, W., Jiang, W., Chen, H., Ding, X., Zhao, H., Zhang, H., *et al.* (2020) 'Coagulopathy and Antiphospholipid Antibodies in Patients with Covid-19.', *The New England journal of medicine*, p. e38. doi: 10.1056/NEJMc2007575.

Zhou, Y., Han, T., Chen, J., Hou, C., Hua, L., He, S., Guo, Y., Zhang, S., Wang, Y., Yuan, J., *et al.* (2020) 'Clinical and Autoimmune Characteristics of Severe and Critical Cases of COVID-19', *Clinical and Translational Science*, 13(6), pp. 1077–1086. doi: 10.1111/cts.12805.

Zohoury, N., Bertolaccini, M. L., Rodriguez-Garcia, J. L., Shums, Z., Ateka-Barrutia, O., Sorice, M., Norman, G. L. and Khamashta, M. (2017) 'Closing the serological gap in the antiphospholipid syndrome: The value of "non-criteria" antiphospholipid antibodies', *Journal of Rheumatology*, 44(11), pp. 1597–1602. doi: 10.3899/jrheum.170044.

Zuo, Y., Estes, S. K., Ali, R. A., Gandhi, A. A., Yalavarthi, S., Shi, H., Sule, G., Gockman, K., Madison, J. A., Zuo, M., *et al.* (2020) 'Prothrombotic autoantibodies in serum from patients hospitalized with COVID-19', *Science Translational Medicine*, 12(570). doi: 10.1126/SCITRANSLMED.ABD3876.

Acknowledgments

We thank Dr. Sumana Srivatsa (former ETH Zurich, now Berkeley, California) for valuable discussions on data models at the initial stage of data exploration, Anne Hollerbach (University Medical Center of the Johannes Gutenberg University, Mainz, Germany) for providing matched plasma and serum samples of aPL-positive patients, and Prof. Dr. Andreas Hierlemann (BEL, D-BSSE, ETH Zurich) for support.

Funding

We acknowledge funding by a grant of the Innovation Fund of the University Hospital Zurich to AA and ME. Institutional core funding by the University of Zurich and the University Hospital of Zurich to AA, as well as Driver Grant 2017DRI17 of the Swiss Personalized Health Network and an Advanced Grant of the European Research Council and a Distinguished Scientist Award of the Nomis Foundation to AA.

Author contributions

Collected and curated biospecimen: ME, DR, MFS, KJL. Conducted the measurements of aPL: KBMF, TB, LR, DR. Established, coordinated, and conducted the high-throughput SARS-CoV-2 antibody serology: ME, AA. Conducted exploratory data analysis: VE, ME, SSK. Developed models for data analysis: SSK. Conducted statistical testing: SSK, VE, ME, DR. Conducted protein similarity analyses: TM. Plotted the data: SSK, VE. Assembled the figures: VE. Wrote the manuscript: ME, VE, SSK, DR, KBMF. All authors revised the first draft of this manuscript and provided critical input.

Competing interests

DR has a management role and is a shareholder of GA Generic Assays GmbH and Medipan GmbH but no financial conflict of interest. Both companies are diagnostic manufacturers. LR and TB are employees of Generic Assays GmbH.

Data and materials availability

Data will be provided upon reasonable request.

Informed Consent Statement

Informed consent was obtained from all subjects involved in the study.

Institutional Review Board Statement

All experiments and analyses involving samples from human donors were conducted with the approval of the local ethics committee (BASEC-Nr. 2020-01731, KEK Zurich; EK2020-16, BTU Cottbus-Senftenberg; reference number 2020-14988-2, ethics committee of the state medical association of Rhineland-Palatinate), in accordance with the provisions of the Declaration of Helsinki and the Good Clinical Practice guidelines of the International Conference on Harmonisation.

Figures and Tables

Figure 1. **Heatmaps and boxplots for IgM and IgG aPL**. **A**. and **B**. Colour-coded representation of IgM (A) and IgG (B) aPL. Higher OD values are evident for AnV, β2, and PT IgM aPL. **C**. and **D**. Boxplot representation of IgM (C) and IgG (D) aPL. Dotted line: OD value 50, a cutoff determined previously by calculating the 99th percentile of 150 apparently healthy individuals (Roggenbuck *et al.*, 2016; Nalli *et al.*, 2018). Pink star: statistically significant distributional differences between non-infected controls and SARS-CoV-2 infected individuals according to Fisher's exact test. Brown star: statistically significant distributional differences between non-infected controls and SARS-CoV-2 infected individuals according to Wilcoxon rank sum test after Benjamini-Hochberg correction. Black dots: Non-infected controls. Turquoise dots: SARS-CoV-2 infected individuals.

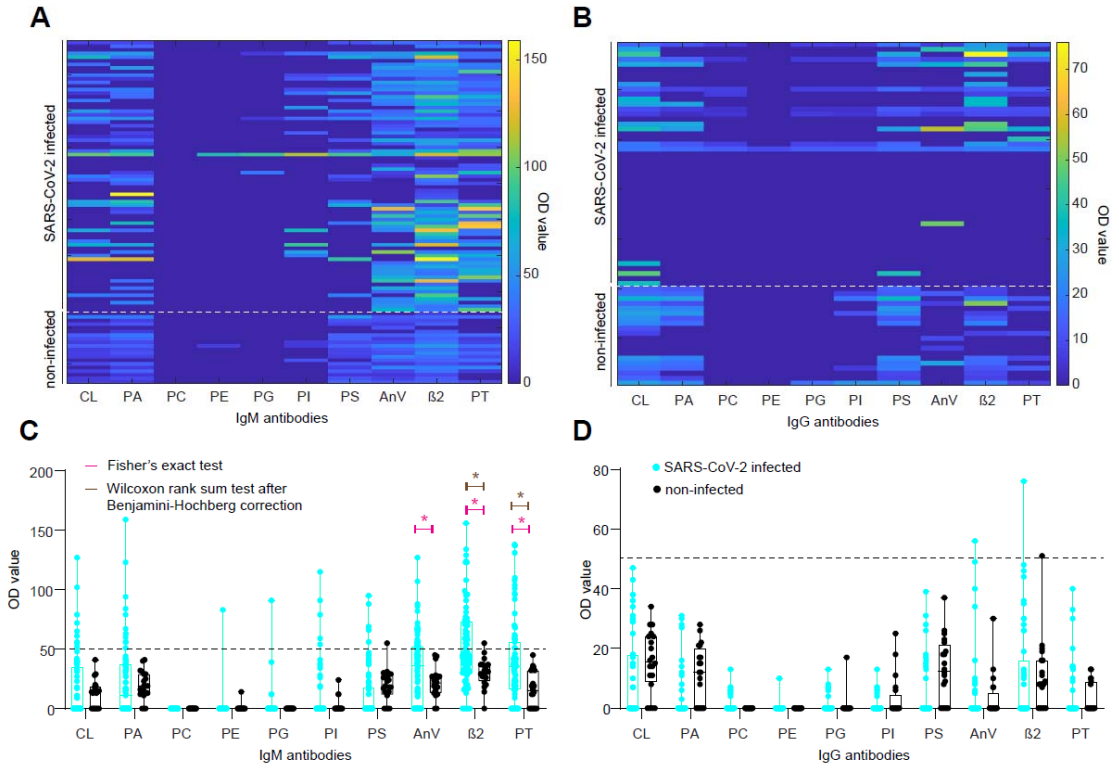

Emmenegger et al. Figure 1

Figure 2. Antibodies against SARS-CoV-2 proteins using a tripartite autoimmune blood immunoassay. **A**. Colour-coded representation of the IgG antibody reactivity profile of non-infected controls and SARS-CoV-2 infected individuals for the SARS-CoV-2 spike protein (S), its receptor
760 binding domain (RBD), and the nucleocapsid protein (NC). The p(EC50) value of the respective sample dilution reflects the inflection point of the logistic regression. **B**. Multicollinearity plot to display the individual reactivity profile of distinct anti-SARS-CoV-2 IgG antibodies. Antibodies against S, RBD, and NC are approximately linear against each other, indicating that information of one is predictive for the other. Bars represent the respective distributions of p(EC50) values obtained for S, RBD, or NC.

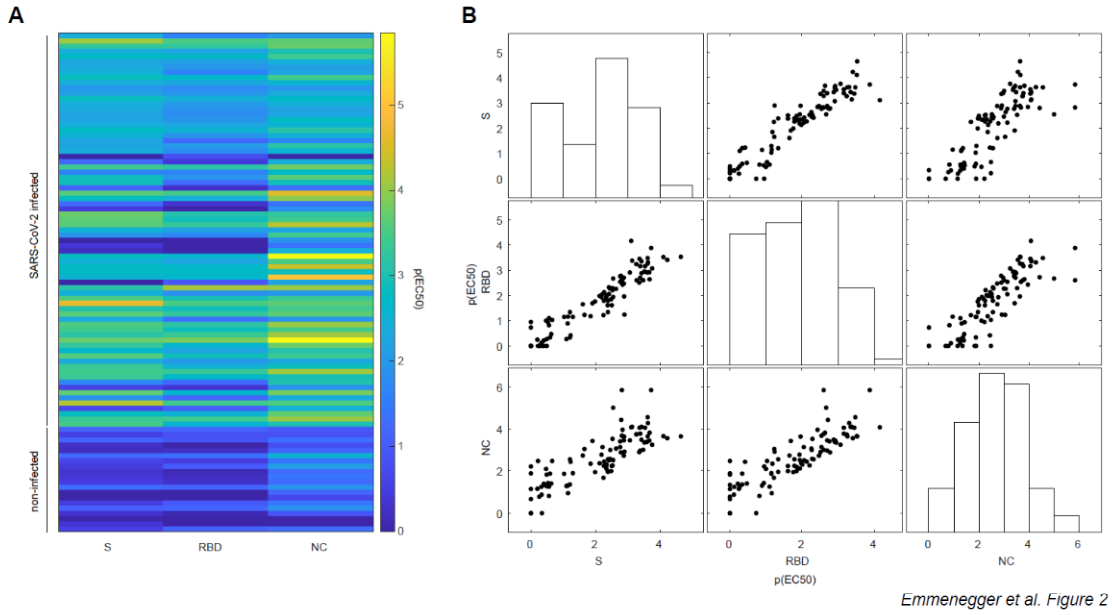

765

Figure 3. **Exploratory multi-parametric data analysis and best-fit model for β2 and PT IgM**. **A**. Data exploration to inspect potential relationships between OD values for PT or β2 IgM with PC1-SARS-CoV-2-IgG, sex (f for female, m for male), disease severity (scores 0-4), days post onset of first disease manifestation, or age (in years). A histogram of OD values was included to display the relative frequencies. After a peak at ca. OD value 40, a second peak at 0 emerges for both PT as well as for β2 IgM. **B**. The fitted vs. observed β2 and PT IgM values. While for β2 IgM, only PC1-SARS-CoV-2-IgG is informative, PC1-SARS-CoV-2-IgG, disease severity, and sex, all contribute to the accurate prediction of OD values of PT IgM. **C**. Same as (B) in the absence of convalescent individuals. **D**. Same as (B) in the absence of non-infected controls.

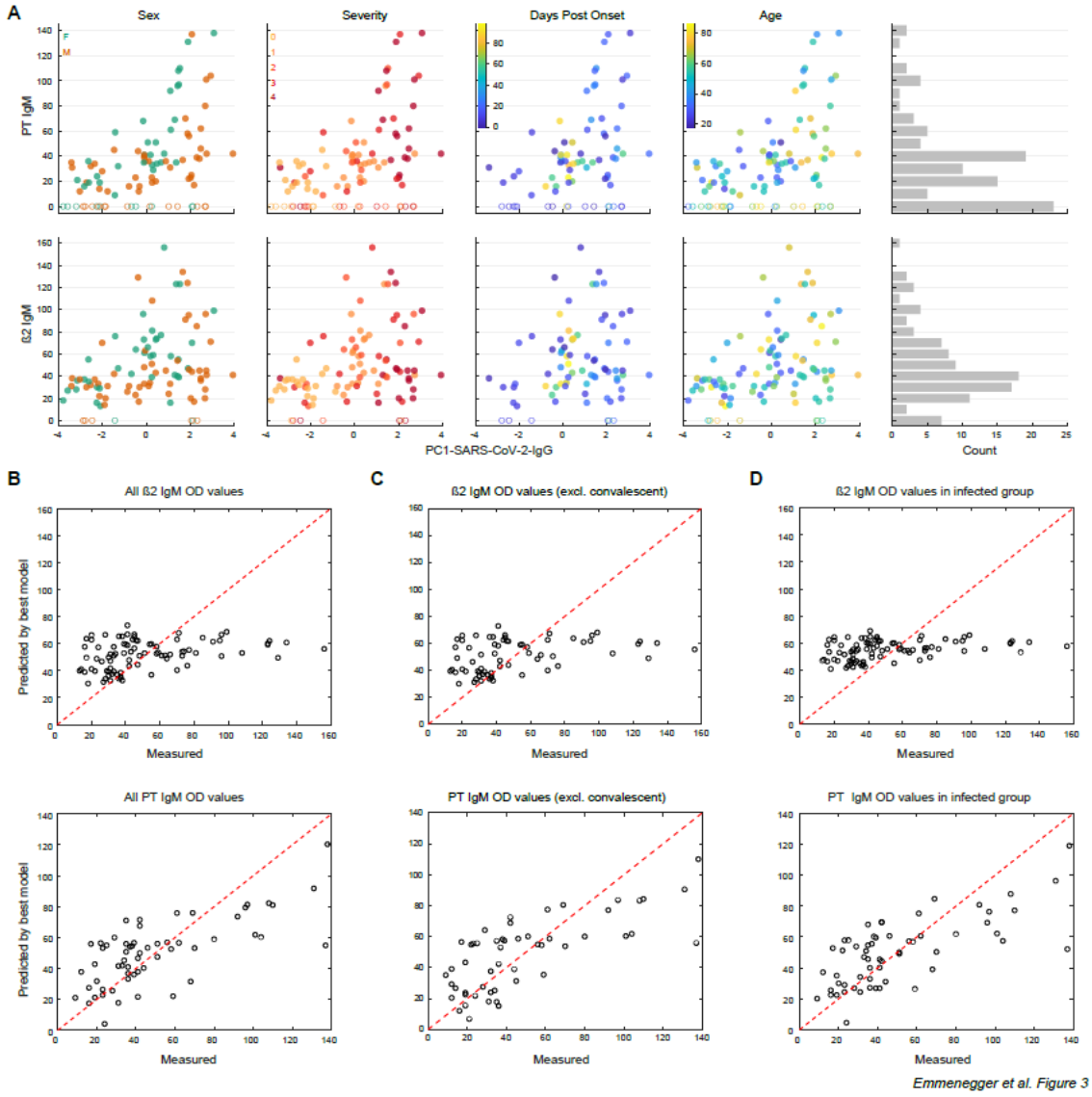

Figure 4. **Sequence analysis of SARS-CoV-2 Spike and human prothrombin**. **A**. Sequence alignments of SARS-CoV-2 Spike (numbering corresponds to UniProt ID P0DTC2) and human prothrombin (P00734). **B**. Cryo-EM structure of trimeric Spike (Protein Data Bank ID 6Z97 (Huo *et al.*, 2020)). Two protomers are shown in surface representation (blue and orange) and one as a grey cartoon with 4 peptide regions shown in red and indicated. Region 3 is located in the receptor-binding domain (RBD). Glycans are not shown for clarity. **C**. Crystal structure of prothrombin (PDB ID 5EDM, (Pozzi *et al.*, 2016)) shown as a cartoon (N-terminus, blue; C-terminus, red). 4 peptide regions are shown in grey and indicated. **D**. Structural superposition of the PRTF motif from Spike and prothrombin.

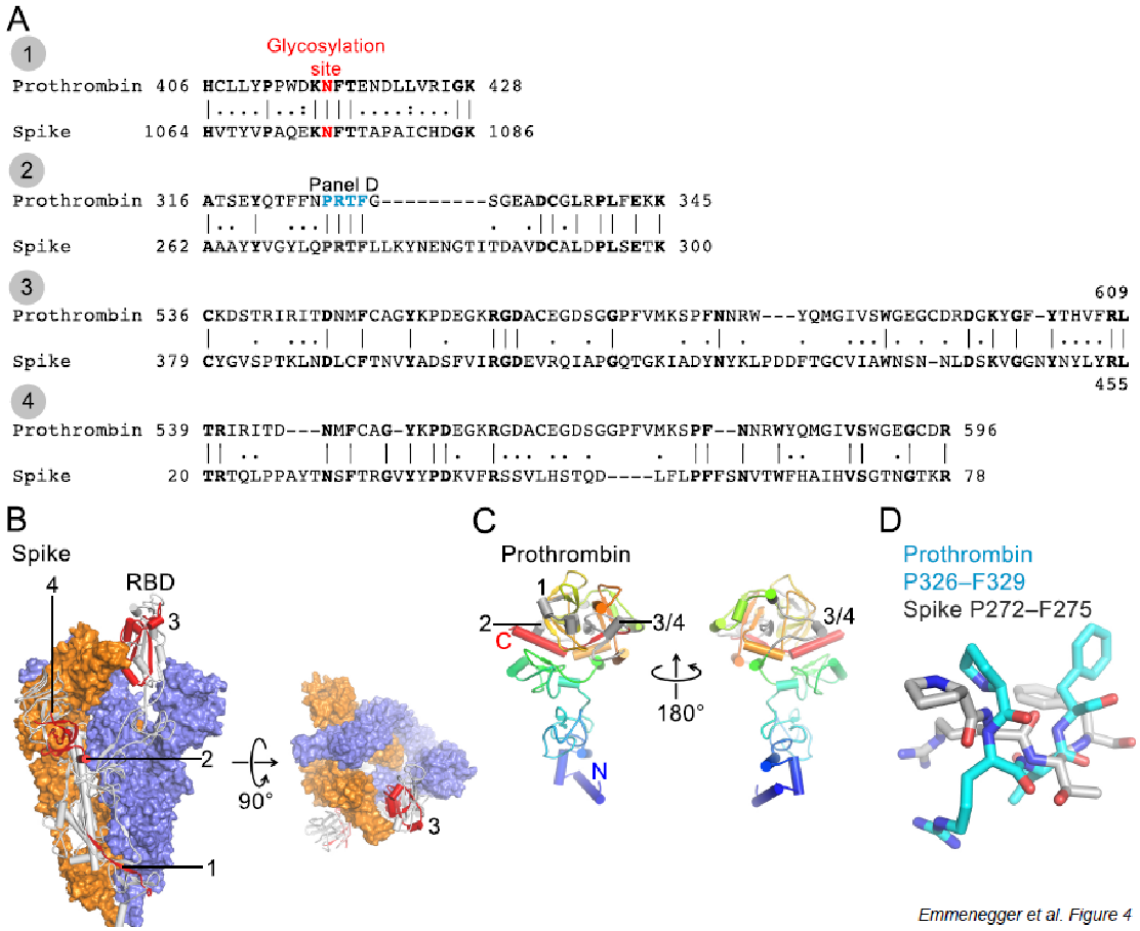

Table 1. Number of samples (N), median age, and sex distribution of non-infected controls and SARS-CoV-2 infected patients (IQR, interquartile range).

Cohort	*n*	*Median age (IQR), years*	*Sex distribution, ratio*
Non-infected controls	20	47 (33-55)	female:male = 45:55
SARS-CoV-2 infected	75	56 (47-70)	female:male = 41:59

790

Table 2. Number of samples (N), severity group, and median day post onset (DPO) of symptom of patients who contracted SARS-CoV-2, belonging to three cohorts (IQR, interquartile range).

Cohort	*N*	*Severity group*	*Median DPO (IQR), days*	*Sample type*
Brandenburg/Saxony	22	1	59 (57-87)	Serum
Mainz	27	2-4	13 (6-20)	Serum
Zurich	26	2-4	12 (8-15)	Heparin plasma

795

Table 3. Overview of antiphospholipid antibodies (aPL) and pair-wise statistical testing (AnV, annexin 5; β2, β2-glycoprotein I, IQR, interquartile range; cardiolipin (CL), OD, optical density; PA, phosphatidic acid; PC, phosphatidylcholine; PE, phosphatidylethanolamine; PG phosphatidylglycerol; PI, phosphatidylinositol; PS, phosphatidylserine; PT, prothrombin).

aPL		***Median (IQR), OD***		***% of individuals above nominal cutoff (OD ≥ 50)***		***p-value (Fisher's exact test)***	***p-value (Wilcoxon rank sum test, Benjamini-Hochberg)***
		Non-infected controls	*SARS-CoV-2 infected*	*Non-infected controls*	*SARS-CoV-2 infected*		
CL	*IgG*	15.5 (9.5,24)	0 (0, 18)	0	0	ns	-
	IgM	14 (0, 18.5)	0 (0, 34)	0	12	ns	-
PA	*IgG*	12(0, 19)	0 (0, 0)	0	0	ns	-
	IgM	19 (12.5, 29)	11 (0, 37)	0	14.67	ns	-
PC	*IgG*	0 (0, 0)	0 (0, 0)	0	0	ns	-
	IgM	0 (0, 0)	0 (0, 0)	0	0	ns	-
PE	*IgG*	0 (0, 0)	0 (0, 0)	0	0	ns	-
	IgM	0 (0, 0)	0 (0, 0)	0	1.33	ns	-
PG	*IgG*	0 (0, 0)	0 (0, 0)	0	0	ns	-
	IgM	0 (0, 0)	0 (0, 0)	0	1.33	ns	-
PI	*IgG*	0 (0, 3)	0 (0, 0)	0	0	ns	-
	IgM	0 (0, 0)	0 (0, 0)	0	6.67	ns	-
PS	*IgG*	12.5 (0, 20.5)	0 (0, 0)	0	0	ns	-
	IgM	18.5 (12.5, 28)	0 (0, 17.5)	5	6.67	ns	-
AnV	*IgG*	0 (0, 3.5)	0 (0, 0)	0	2.04	ns	-
	IgM	21.5 (13, 27)	36 (0, 52)	0	29.33	0.0026	ns
β2	*IgG*	8 (0, 16)	0 (0, 14.5)	5	2.04	ns	-
	IgM	31 (24, 37)	45 (30.25, 72.5)	5	42.67	0.0012	0.005
PT	*IgG*	0 (0, 8.5)	0 (0, 0)	0	0	ns	-

IgM	15 (0, 32)	35 (16, 54.75)	0	28	0.0052	0.005

Supplementary Figures

Figure S1. **Demographic features of non-infected controls and SARS-CoV-2 infected individuals**. **A**. Age distribution of entire cohort for non-infected controls (orange) and SARS-CoV-2 infected individuals (blue). The distribution of the controls indicates a generally younger age versus the SARS-CoV-2 infected individuals. **B**. Sex distribution of entire cohort for non-infected controls (orange) and SARS-CoV-2 infected individuals (blue). The distribution in both cohorts was slightly skewed towards males versus females.

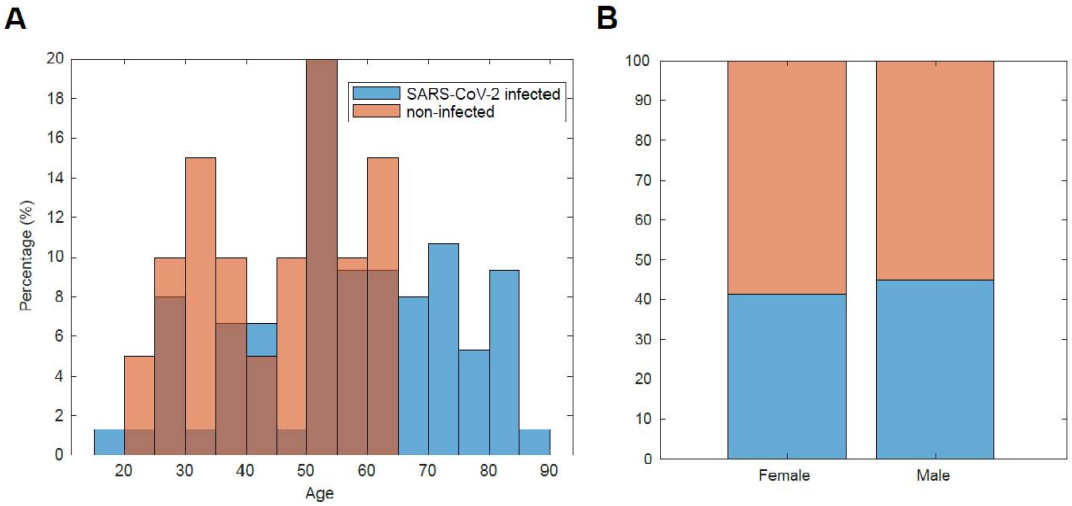

Figure S2. **LIA comparison of serum and plasma samples and UMAP representation of aPL profiles**. **A**. Comparison of patient-matched serum and plasma samples with LIA technology using linear regression. Pearson correlation coefficient is 0.9974 (95% confidence intervals: 09611-1.034) and R^2 of 0.9813. **B**. Same as above, visualised as Bland-Altman plot. Bland-Altman analysis indicated a bias of -2.717 (95% confidence interval: -17.53-12.1). Measurements (for A and B) were done as unicates for the entire LIA panel. **C**. and **D**. UMAP of IgM aPL do not reveal any clear cluster between non-infected (black) and SARS-CoV-2 infected (turquoise) individuals, both for IgM (A) as well as for IgG (B) aPL.

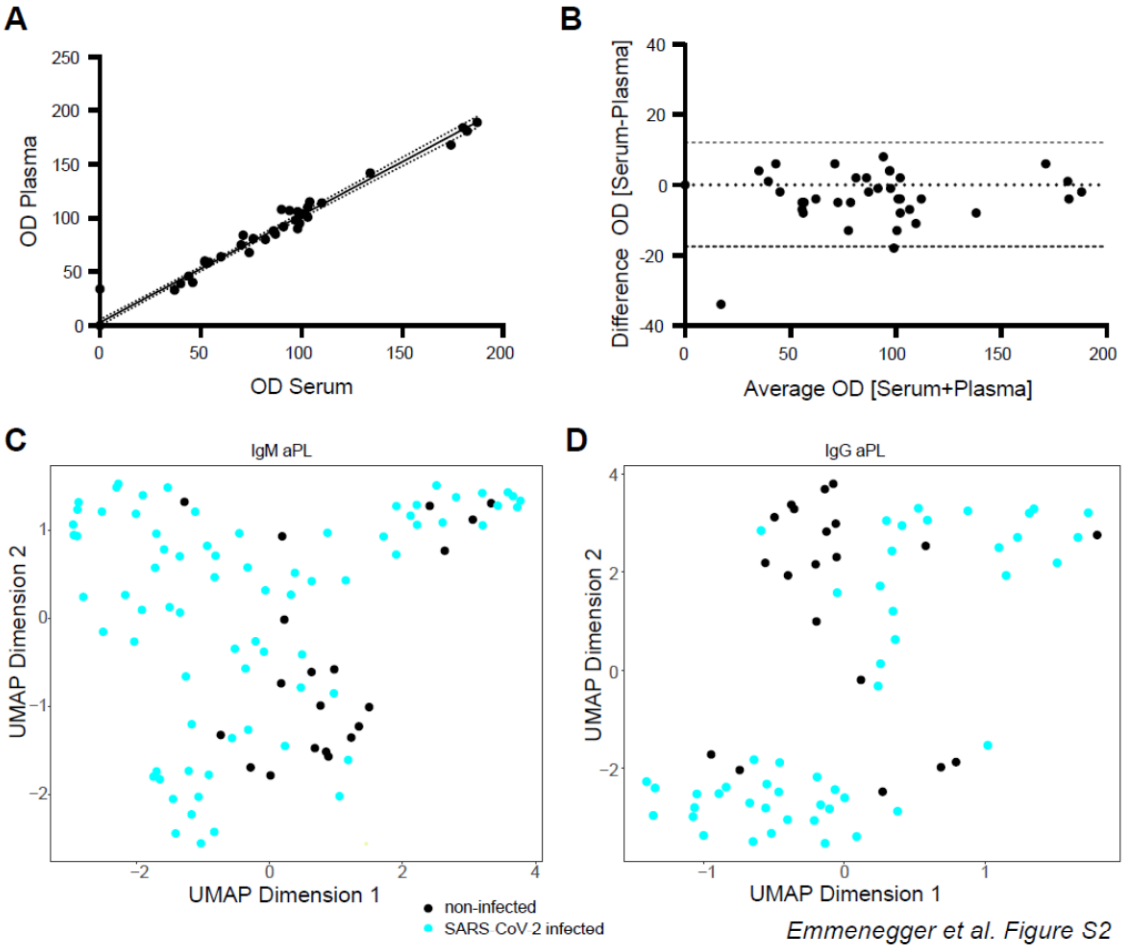

Emmenegger et al. Figure S2

Figure S3. **TRABI comparison of serum and plasma and UMAP representation of SARS-CoV-2 IgG profiles**. **A**. Binding curves of patient-matched serum and plasma samples. Three SARS-CoV-2 proteins were used to conduct the tripartite-autoimmune blood immunoassay technology: the SARS-CoV-2 spike ectodomain (S), its receptor binding domain (RBD), and the nucleocapsid protein (NC). All samples were tested as technical duplicates and are shown as mean with standard deviation. **B**. Based on the binding curves, the concentration at half-maximum binding of the sigmoidal curve, or the p(EC50) value, was calculated. p(EC50) values for S, RBD, and NC for all patients are compared in a scatter plot with serum-based p(EC50) values on the x-axis and plasma-based p(EC50) values on the y-axis. The Pearson correlation coefficient was 0.9942 (95% confidence interval: 0.9865-0.9975) and R^2 was 0.9885. Dotted line represents the 95% confidence interval of the linear regression. **C**. Visualisation of the same data as shown in (B) using a Bland-Altman plot. Bias was calculated to be 0.01976 with a standard deviation of 0.1361. Dotted lines represent the confidence intervals (-0.2471 to 0.2866). **D**. UMAP representation of anti-SARS-CoV-2 protein antibodies displays clear clusters, with non-infected controls (black) and non-IgG-reactive SARS-CoV-2 infected individuals (turquoise) clustering separately from IgG-reactive SARS-CoV-2 infected individuals.

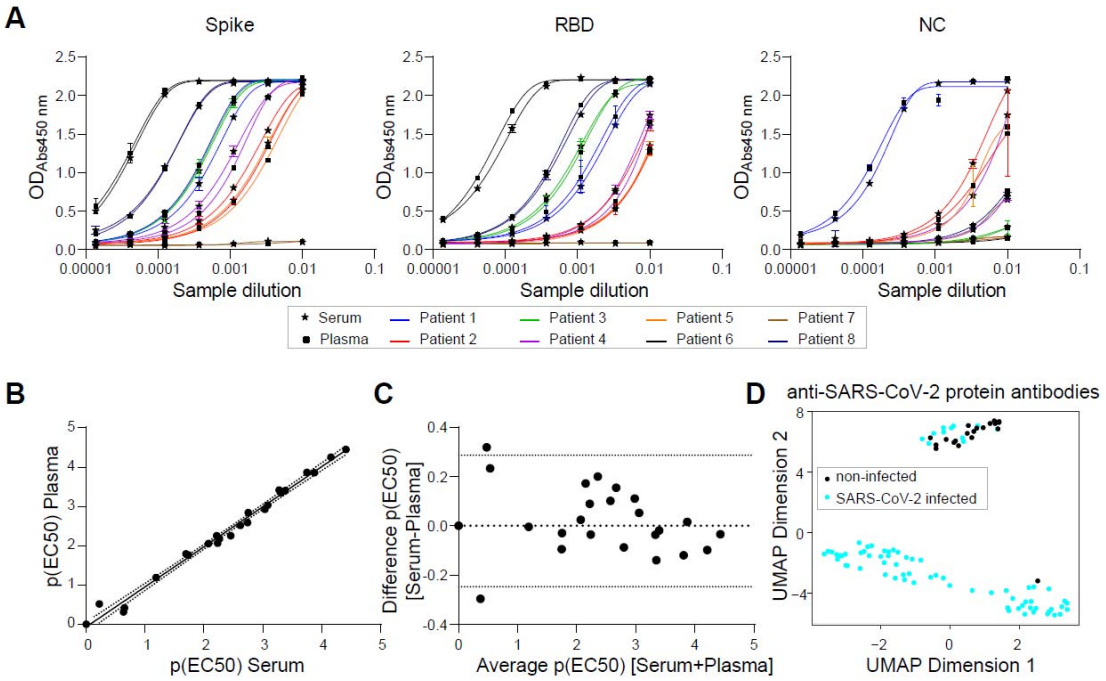

Emmenegger et al. Figure S3

Table S1. Equation and performance characteristics of multiple linear fixed-effect and mixed-effect models using data from non-infected controls and SARS-CoV-2 infected individuals. The best model is shown in bold letters (AIC, Akaike information criterion; β2, β2-glycoprotein I; DPO, day post onset; PC, principal component).

Equation	AIC	Log-likelihood	R^2_{adj}	Likelihood ratio (p-value)
β2 IgM ~ 1	855.08	-426.54	0	-
β2 IgM ~ 1 + PC1-SARS-CoV-2-IgG	845.76	-420.88	0.110	11.32 (<0.001)
β2 IgM ~ 1 + PC1-SARS-CoV-2-IgG + (1 | Sex)	849.76	-420.88	0.110	0 (ns)
β2 IgM ~ 1 + PC1-SARS-CoV-2-IgG + (PC1-SARS-CoV-2-IgG - 1 | Sex)	849.76	-420.88	0.110	0 (ns)
β2 IgM ~ 1 + severity + PC1-SARS-CoV-2-IgG	849.69	-420.84	0.101	0.78 (ns)
β2 IgM ~ 1 + Age + PC1-SARS-CoV-2-IgG	849.16	-420.58	0.106	0.6 (ns)
β2 IgM ~ 1 + DPO + PC1-SARS-CoV-2-IgG	681.23	-336.61	0.003	168.53 (<0.001)
PT IgM ~ 1	700.69	-349.35	0	-
PT IgM ~ 1 + PC1-SARS-CoV-2-IgG	678.15	-337.08	0.279	24.5 (<0.001)
PT IgM ~ 1 + PC1-SARS-CoV-2-IgG + (1 | Sex)	677.29	-334.64	0.353	4.87 (0.027)
PT IgM ~ 1 + PC1-SARS-CoV-2-IgG + (1 | Sex) + (PC1-SARS-CoV-2-IgG -1| Sex)	675.09	332.55	0.417	4.19 (0.041)
PT IgM ~ 1 + PC1-SARS-CoV-2-IgG + severity + (1 | Sex) + (PC1-SARS-CoV-2-IgG -1| Sex)	674.52	331.26	0.433	2.57 (ns)
PT IgM ~ 1 + PC1-SARS-CoV-2-IgG + severity + Age + (1 | Sex) + (PC1-SARS-CoV-2-IgG -1| Sex)	673.41	329.71	0.450	5.68 (ns)
PT IgM ~ 1 + PC1-SARS-CoV-2-IgG + DPO + (1 | Sex) + (PC1-SARS-CoV-2-IgG -1| Sex)	559.16	273.58	0.439	117.94 (<0.001)

Table S2. Equation and performance characteristics of multiple linear fixed-effect and mixed-effect models using data from non-infected controls and SARS-CoV-2 infected individuals, without including data from convalescent individuals. The best model is shown in bold letters (AIC, Akaike information criterion; DPO, day post onset; PC, principal component; PT, prothrombin).

Equation	AIC	Log-likelihood	R^2_{adj}	Likelihood ratio (p-value)
β2 IgM ~ 1	658.50	-328.25	0	-
β2 IgM ~ 1 + PC1-SARS-CoV-2-IgG	650.87	-323.43	0.134	9.63 (0.002)
β2 IgM ~ 1 + PC1-SARS-CoV-2-IgG + (1 | Sex)	654.87	-323.43	0.121	0 (ns)
β2 IgM ~ 1 + PC1-SARS-CoV-2-IgG + (PC1-SARS-CoV-2-IgG - 1 | Sex)	656.87	-323.43	0.121	0 (ns)
β2 IgM ~ 1 + severity + PC1-SARS-CoV-2-IgG	658.84	-323.42	0.107	0.03 (ns)
β2 IgM ~ 1 + Age + PC1-SARS-CoV-2-IgG	659.84	-322.92	0.106	1.02 (ns)
β2 IgM ~ 1 + DPO + PC1-SARS-CoV-2-IgG	483.6	-235.80	0.1	175.27 (<0.001)
PT IgM ~ 1	517.13	-257.56	0	-
PT IgM ~ 1 + PC1-SARS-CoV-2-IgG	498.56	-247.28	0.313	20.57 (<0.001)
PT IgM ~ 1 + PC1-SARS-CoV-2-IgG + (1 | Sex)	499.75	-245.88	0.38	2.80 (ns)
PT IgM ~ 1 + PC1-SARS-CoV-2-IgG + (1 | Sex) + (PC1-SARS-CoV-2-IgG -1 | Sex)	496.9	-243.45	0.48	7.66 (0.006)
PT IgM ~ 1 + PC1-SARS-CoV-2-IgG + severity + (1 | Sex) + (PC1-SARS-CoV-2-IgG -1 | Sex)	498.86	-243.43	0.47	0.04 (ns)
PT IgM ~ 1 + PC1-SARS-CoV-2-IgG + severity + Age + (1 | Sex) + (PC1-SARS-CoV-2-IgG -1 | Sex)	497.77	-241.88	0.49	3.13 (ns)
PT IgM ~ 1 + PC1-SARS-CoV-2-IgG + DPO + (1 | Sex) + (PC1-SARS-CoV-2-IgG -1 | Sex)	384.96	-186.48	0.40	113.94 (<0.001)

Table S3. Equation and performance characteristics of multiple linear fixed-effect and mixed-effect models using data from SARS-CoV-2 infected individuals without the non-infected controls. The best model is shown in bold letters (AIC, Akaike information criterion; DPO, day post onset; PC, principal component; PT, prothrombin).

Equation	AIC	Log-likelihood	R^2_{adj}	Likelihood ratio (p-value)
β2 IgM ~ 1	677.5	-337.75	0	-
β2 IgM ~ 1 + PC1-SARS-CoV-2-IgG	677.39	-336.70	0.015	2.10 (ns)
β2 IgM ~ 1 + PC1-SARS-CoV-2-IgG + (1 | Sex)	681.50	-337.75	0.000	0 (ns)
β2 IgM ~ 1 + PC1-SARS-CoV-2-IgG + (PC1-SARS-CoV-2-IgG | Sex)	681.40	-336.7	0.016	2.10 (ns)
β2 IgM ~ 1 + severity + PC1-SARS-CoV-2-IgG	680.46	-336.23	0.014	3.04 (ns)
β2 IgM ~ 1 + Age + PC1-SARS-CoV-2-IgG	681.16	-336.58	0.004	2.34 (ns)
β2 IgM ~ 1 + DPO + PC1-SARS-CoV-2-IgG	681.23	-336.61	0.003	2.27 (ns)
PT IgM ~ 1	578.95	-288.48	0	-
PT IgM ~ 1 + PC1-SARS-CoV-2-IgG	565.83	-280.91	0.213	15.13 (<0.001)
PT IgM ~ 1 + PC1-SARS-CoV-2-IgG + (1 | Sex)	563.67	-277.83	0.328	6.16 (0.013)
PT IgM ~ 1 + PC1-SARS-CoV-2-IgG + (1 | Sex) + (PC1-SARS-CoV-2-IgG -1| Sex)	561.19	-275.6	0.402	4.48 (0.034)
PT IgM ~ 1 + PC1-SARS-CoV-2-IgG + severity + (1 | Sex) + (PC1-SARS-CoV-2-IgG -1| Sex)	558.67	-273.34	0.446	4.52 (0.033)
PT IgM ~ 1 + PC1-SARS-CoV-2-IgG + severity + Age + (1 | Sex) + (PC1-SARS-CoV-2-IgG -1| Sex)	557.93	-271.97	0.464	2.74 (ns)
PT IgM ~ 1 + PC1-SARS-CoV-2-IgG + DPO + (1 | Sex) + (PC1-SARS-CoV-2-IgG -1| Sex)	560.14	-273.07	0.442	0.53 (ns)